Materials Science and Engineering A 553 (2012) 51–58

Contents lists available at SciVerse ScienceDirect

Materials Science and Engineering A

journal homepage: www.elsevier.com/locate/msea

Microstructure and fatigue performance of single and multiple linear fiber laser welded DP980 dual-phase steel

W. Xu[a], D. Westerbaan[b], S.S. Nayak[b], D.L. Chen[a,*], F. Goodwin[c], E. Biro[d], Y. Zhou[b]

[a] Department of Mechanical and Industrial Engineering, Ryerson University, 350 Victoria Street, Toronto, Ontario M5B 2K3, Canada
[b] Department of Mechanical and Mechatronics Engineering, University of Waterloo, 200 University Avenue West, Waterloo, Ontario N2L 3G1, Canada
[c] International Zinc Association, Durham, NC 27713, USA
[d] ArcelorMittal Global Research, Hamilton, Ontario L8N 3J5, Canada

ARTICLE INFO

Article history:
Received 7 April 2012
Received in revised form 26 May 2012
Accepted 28 May 2012
Available online 4 June 2012

Keywords:
Laser welded blank
DP980 dual-phase steel
Fiber laser welding
Diode laser welding
Microstructure
Fatigue

ABSTRACT

The aim of this study was to identify the effect of fiber laser welding (FLW) on the microstructure, hardness, tensile properties and fatigue performance of high-strength (UTS ≥ 980 MPa) DP980 dual-phase steel with single linear and multiple linear joint geometry. While FLWed joints showed tempered martensite at the outer heat-affected zone (HAZ) which caused softening in the welds, a lower extent of martensite tempering and higher hardness value were observed in the narrower HAZ of the FLWed joint than in the wider HAZ of the diode laser welded (DLWed) joint due to a higher power density, faster welding speed, lower heat input, and faster cooling rate. A characteristic "suspension bridge"-like hardness profile with the fusion zone (FZ) hardness as a "pylon" appeared in the FLW due to the formation of almost fully martensitic structure in the FZ. Despite the lower ductility after FLW, a joint efficiency of about 96–97% was achieved with the yield strength essentially unchanged. At higher stress amplitudes, fatigue life of the FLWed joints was equivalent to that of BM, but at lower stress amplitudes no direct improvement in the fatigue resistance was observed due to the presence of soft zone and weld concavity. Multiple linear welds appeared to increase the probability of premature dynamic fatigue failure at lower stress amplitudes as a result of increasing number of weld concavities and soft zones. Fatigue crack initiation occurred from the specimen surface where the weld concavity met with a soft zone, and crack propagation was mainly characterized by the typical fatigue striations along with secondary cracks.

1. Introduction

Lasers have played an important role in the joining of materials since the invention of high power gas and solid state lasers in the 1960s [1–5]. Laser welding is an enabling technology which is fast and precise in joining a wide variety of materials with varying thicknesses and types [6–9]. Several types of laser welding are used today in the automotive, aerospace, shipment, semiconductor, medical and jewelry industries, such as Nd:YAG laser welding, CO_2 laser welding, and diode laser welding (DLW) [10]. To reduce cost, material consumption and vehicle component weight, and increase fuel efficiency, laser welded blank (LWB), with an innovative idea of joining two or more sheets having different thicknesses, mechanical properties, or surface coatings together via laser welding, has been increasingly used in the automotive sector [11–14].

Another strategy that car makers are using to construct lighter motor vehicles is the ever-increasing use of the advanced high strength steel (AHSS) such as dual-phase (DP) steel for automotive body fabrication [15–22]. DP steels are a family of steels with a composite microstructure made of islands of martensite and sometimes bainite in the ferrite matrix. This microstructure provides the material with a higher initial work hardening rate and excellent uniform and total elongations to give DP steels a much higher ultimate tensile strength (UTS) and a lower yield strength (YS)-to-UTS ratio compared to the conventional steels with similar strengths. These characteristics have made DP steels attractive for automotive applications [7,15,23–25].

While the LWB is viable for the lower and intermediate grades of DP steels, e.g., DP350 and DP600 steels as well as high-strength low-alloy (HSLA) steels, it is fairly challenging for the higher grade of DP980 steel using laser welding. Previous studies on DP steels showed that the welding led to the formation of a soft zone in the sub-critical area of the heat-affected zone (HAZ), and the mechanical properties and formability of the welded joints were significantly affected by the presence of this area [13,20,21,25–30]. For example, Farabi et al. [20,26–28] have recently studied microstructure and mechanical properties of similar and dissimilar DLWed joints in DP600 and DP980 and observed

* Corresponding author. Tel.: +1 416 979 5000x6487; fax: +1 416 979 5265.
E-mail address: dchen@ryerson.ca (D.L. Chen).

0921-5093/$ – see front matter © 2012 Elsevier B.V. All rights reserved.
http://dx.doi.org/10.1016/j.msea.2012.05.091

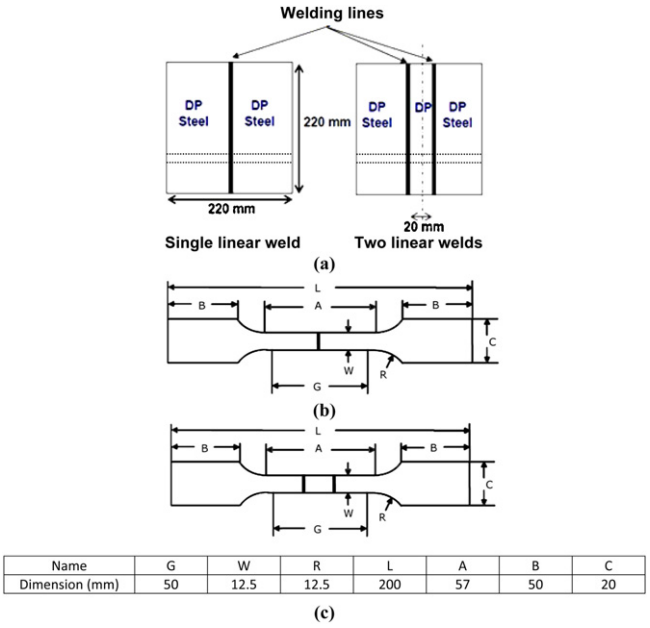

Name	G	W	R	L	A	B	C
Dimension (mm)	50	12.5	12.5	200	57	50	20

Fig. 1. Geometry and dimensions of work pieces and test specimens, (a) work pieces to be welded, (b) tensile and fatigue test samples cut from the single linear weld indicated by the dashed lines at the left side of (a), (c) tensile and fatigue test samples cut from the multiple linear weld indicated by the dashed lines at the right side of (a).

a significant change in the microstructure and hardness in the HAZ and fusion zone (FZ), which caused a reduction of the tensile and fatigue performance. To reduce or minimize the effect of the soft zone on the mechanical properties, a newer type of fiber laser, which was first used in materials processing in 2000 [31], is promising for joining the stronger grades of automotive steels because of its multiple advantages such as high power density, efficiency, compact design, good quality, and a robust setup for mobile applications compared with Nd:YAG laser welding, CO_2 laser welding and DLW [26,28,32–37]. However, like other types of laser welding processes, fiber laser welding (FLW) is expected to result in a softened zone in the HAZ as well as change in the microstructural heterogeneity, which would subsequently affect the mechanical properties and structural integrity. Little is known about the critical structural integrity and durability of FLWed joints under dynamic or cyclic loading since no studies on the cyclic performance of FLWed DP980 steel have been reported in the literature. It is unclear how severely the microstructure would change after FLW in comparison with the DLW, and if multiple laser welds would affect the fatigue life of a LWB. This study was, therefore, aimed at evaluating the microstructural changes and fatigue resistance of FLWed blanks with single (FLW-S) and multiple (FLW-M) welds of a DP980 steel, in comparison with those from the DLWed blanks.

2. Material and experimental procedure

DP980 dual-phase steel with a composition (in wt.%) of 0.15 C, 1.5 Mn, 0.31 Si, 0.05 Al, and in the form of 1.2 mm thick sheet with hot dip galvannealing (GA) coating was selected in the present study. The geometry and dimensions of the metal sheets prepared for welding are shown in Fig. 1(a). Laser welding was conducted using a Nuvonyx diode laser system and an IPG Photonics YLS-6000 fiber laser system, with the welding parameters used to fabricate the LWB shown in Table 1. The fiber laser system possessed a fiber core diameter of 0.3 mm and welding was performed with a head angle of 0° (i.e., the laser beam was perpendicular to the surface of work pieces); no shielding gas was used during the welding process. The metallographic samples for the microstructural examination were cut from the weld cross-section, then mounted, ground, polished, and etched with a 2% Nital solution. The etched samples were observed using a light microscope in conjunction with a Clemex image analysis system and JEOL 6380LV scanning electron microscope (SEM), equipped with Oxford energy dispersive X-ray spectroscopy (EDS) and three-dimensional fractographic analysis tool. Vickers microhardness was determined from the polished samples across the weld using a computerized microhardness tester at a load of 200 g and a dwell time of 15 s. All indentations were adequately spaced to prevent any potential effect of strain fields caused by adjacent indentations. Prior to the microhardness tests on the polished welded joints, two calibration tests were done using a standard reference test block to ensure the correctness of the measured hardness values.

Tensile and fatigue test samples following ASTM-E8M standard with the geometry and dimensions shown in Fig. 1 were sectioned from the welded work pieces with the weld positioned at the center of gauge length for the single linear weld (Fig. 1(b)), or two welds located within the gauge length which were symmetrical with respect to the center of the sample (Fig. 1(c)). Tensile tests were carried out using a fully computerized United tensile testing machine at room temperature and strain rates from 1×10^{-5} to 1×10^{-2} s^{-1}. An extensometer with a gauge length of 50 mm and a strain limit of 20% was used to measure the strain during the tensile tests. Fatigue tests were conducted on a fully computerized Instron 8801 servo-hydraulic testing system under load control. To avoid the occurrence of buckling for such welded thin sheets, tension-tension cyclic loading at a stress ratio of $R = 0.1$ was applied at a frequency of 50 Hz and sinusoidal waveform. The fatigue fracture surfaces were examined via a SEM to identify fatigue crack initiation sites and crack propagation mechanisms.

3. Results and discussion

3.1. Microstructure

The overall weld cross-section profile and microstructural changes across a DLWed and a FLWed DP980 joints are shown in Figs. 2 and 3, respectively. It is seen that the cross-section of the welds (Figs. 2(a) and 3(a)) exhibited a significant microstructural change in the HAZ and FZ for both welded joints. The width of HAZ for the DLWed DP980 joint (on average ~2 mm) was much wider than that of the FLWed DP980 joint (~0.4 mm). Similarly, the width of the FZ for the DLWed DP980 joint was approximately 3 mm, which was about six-fold wider than that of the FLWed DP980 joint (~0.5 mm on average), as seen in Figs. 2(a) and 3(a). Similar results have been observed by Chowdhury et al. [38–40], where the width of HAZ and FZ after FLW was much smaller than that after DLW or double-sided arc welding in an AZ31B-H24 magnesium alloy. The reason for the narrower HAZ and FZ in the FLW was attributed to its considerably smaller laser beam size (0.28 mm^2 for the FLW versus 10.8 mm^2 for the DLW, Table 1) and the resultant high power density, which allowed it to weld at a much faster speed and at a lower heat input than the DLW [21].

More detailed microstructural changes could be seen in (b)–(d) of Figs. 2 and 3. It is seen from Figs. 2(b) and 3(b) that DP980 base metal (BM) consisted of typical martensite in the ferrite matrix, where the volume fraction of martensite was determined by a direct image analysis tool in SEM to be approximately 0.56. Similar microstructural characteristics in the high-strength DP980 dual-phase steel have also been observed with a volume fraction of martensite being 0.52, 0.50 and 0.55, respectively [20,25,41]. It should be noted that both images on the BM shown in Figs. 2(b) and 3(b) were aimed to indicate that the same material was used in

Table 1
Details of the DLW and FLW parameters used for joining DP980 steel in the present study.

Laser system	Laser source	Laser power (kW)	Welding speed (m/min)	Focal length (cm)	Beam dimension (mm)
Nuvonyx ISL-4000	Diode	4	1	9	12 × 0.9
IPG Photonics YLS-6000	Fiber	6	16	30	0.6 (spot size in diameter)

both the FLW and DLW. Microstructural examination of the HAZ of both DLWed and FLWed joints revealed the presence of tempered martensite in the ferrite matrix, as shown in Figs. 2(c) and 3(c), respectively, where some extent of decomposition of the originally existing martensite in the BM (Figs. 2(b) and 3(b)) could clearly be seen. Tempered martensite and the associated HAZ-softened zone in the laser welded DP980 steel have been reported in the earlier studies [20,26,27,30,42]. The temperature experienced in the HAZ-softened region was close to or below the critical temperature (A_{c1} at which austenite begins to form during heating) during welding, leading to a tempering effect in which the martensite phase present in the BM decomposed [20,23,26,27,30,42–44]. The microstructure of tempered martensite typically consisted of very small and uniformly dispersed cementite (Fe_3C) particles embedded within a continuous ferrite matrix. As seen in Figs. 2(c) and 3(c) only partial tempering occurred in the HAZ after the FLW. It is of interest to observe that more martensite decomposition occurred in the HAZ of the DLWed joint than in the HAZ of the FLWed joint, as compared Fig. 2(c) with Fig. 3(c). This was due to the fact that a much longer welding time arising from a much lower welding speed (16 m/min in the DLW vs. 1 m/min in the FLW, as seen in Table 1), in conjunction with an overall more heat input as indicated by the considerably wider FZ and HAZ after DLW (Fig. 2(a)), resulted in a more complete martensite tempering/decomposition in the DLW process. Similarly, the Nd:YAG laser welds also exhibited less tempering than diode laser welds [21]. This was also true in the resistance spot welding where the cooling rate was much faster [44]. The final microstructures in the FZ also depended on the heat input and cooling rate, based upon a continuous-cooling transformation (CCT) diagram of low carbon steel, where the microstructure could contain a combination of grain boundary ferrite, side-plate ferrite, accicular ferrite, bainite and martensite as the FZ was cooled down to room temperature [45]. The SEM micrographs shown in Fig. 2(d) clearly showed such a microstructural feature consisting mainly of martensite, bainite and ferrite in the FZ of DLW. However, the FZ of the FLWed joint exhibited almost a fully martensitic structure (Fig. 3(d)). While the FLW process had a higher power density than the DLW process, the cooling rate in the FZ of the FLWed joint was appreciably faster, due to the 16 times faster welding speed (Table 1) and much smaller FZ (Fig. 3(a)) in the FLW process. As discussed above, according to a CCT diagram of weld metal of low carbon steel [45], the

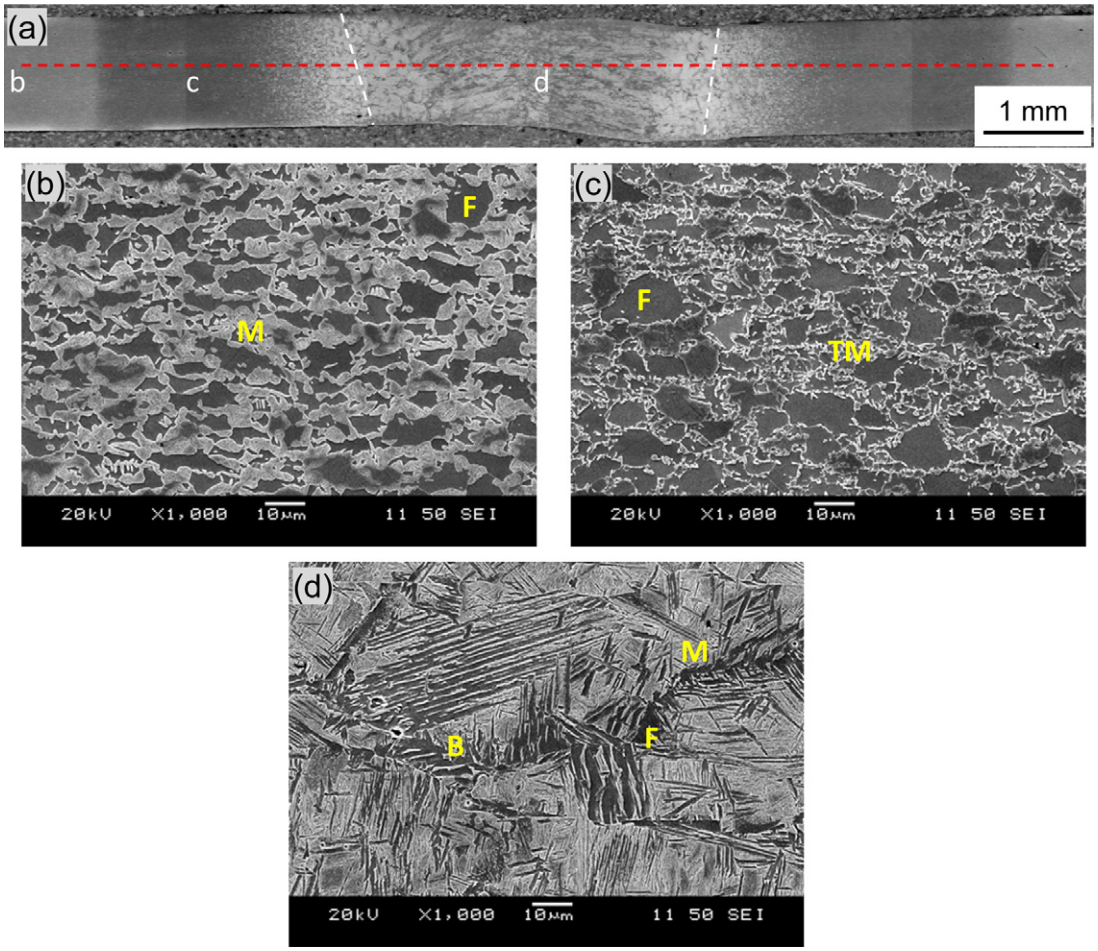

Fig. 2. Micrographs showing the microstructure change of a DLWed DP980 steel joint, (a) overall view of the cross section, (b) DP980 BM, (c) HAZ (soft zone), (d) FZ (where M: martensite, TM: tempered martensite, B: Bainite, and F: ferrite).

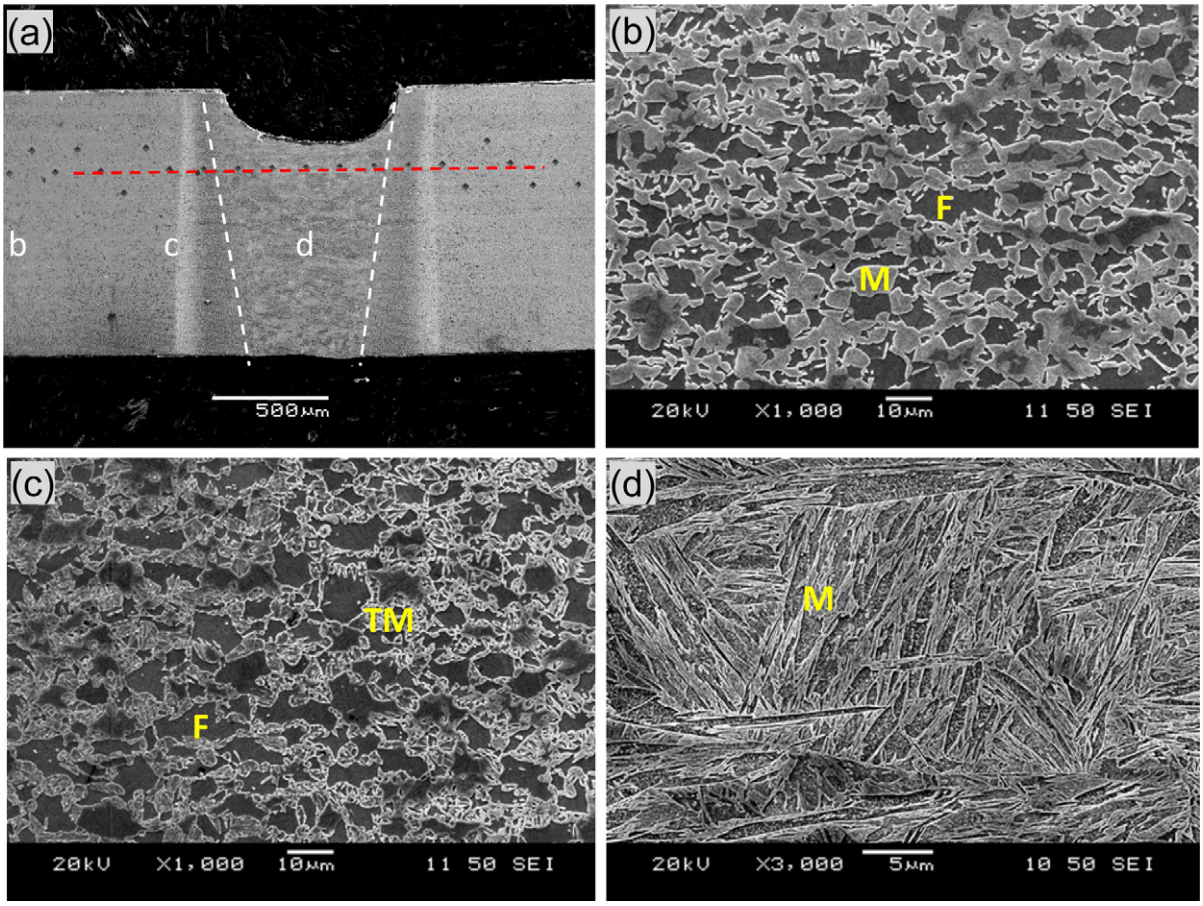

Fig. 3. Micrographs showing the microstructure change of a FLWed DP980 steel joint, (a) overall view of the cross section, (b) DP980 BM, (c) HAZ (soft zone), (d) FZ (where M: martensite, TM: tempered martensite, and F: ferrite).

thermal history path would move downward steeply at a rapid cooling rate missing the pearlite and bainite noses of the curve, so that the martensite start temperature would be directly reached. This means that there would be no chance to form other microstructure but possibly only maternsite in the FZ of FLWed joint, as shown in Fig. 3(d). Sreenivasan et al. [21] reported a similar result for a 3 kW Nd:YAG laser welding applied on the DP980 steel sheets with a thickness of 1.17 mm.

3.2. Hardness profiles

Vickers microhardness profiles across the welds of the DLWed joint and the FLW-S joint (as indicated by the dashed lines in Figs. 2(a) and 3(a)) are shown in Fig. 4. The hardness value in the DP980 BM was determined to be approximately 350–360 HV, which could be seen from the hardness profile of the FLW-S joint. After welding the hardness became obviously higher in the FZ of both DLWed and FLWed joints, and soft zones occurred beside the FZ in both types of laser welded joints (Fig. 4). However, the hardness in the FZ was much higher in the FLWed joint (~480 HV) than in the DLWed joint (~340 HV) due to the formation of predominantly martensitic structure in the FZ of FLWed joint (Fig. 3(d)) with respect to the co-existence of martensite, ferrite and bainite in the FZ of DLWed joint (Fig. 2(d)). It is clear that the soft zone of FLWed joint was substantially narrower than that of DLWed joint. Besides, the former had a higher minimum hardness valley of about 280 HV than the latter (~200 HV). This was a consequence of a milder extent of tempering or decomposition of pre-existing martensite in the DP980 steel in the FLWed joint (Fig. 3(c)) than in the DLWed joint (Fig. 2(c)), stemming from a faster welding speed and cooling rate in the FLW process, since the tempered martensite had a lower hardness or strength than the normal martensite with a body-centered tetragonal (BCT) structure.

Fig. 5 shows the microhardness profile across the weld of a FLWed multiple linear joint. Each weld bead in the FLWed multiple linear joint had a similar result to that in the FLWed single linear joint (Fig. 4), i.e., with a FZ hardness of ~480 HV and an average soft zone hardness of ~280 HV. The only difference lay in that the multiple linear FLWed joint had four soft zones located at both sides of

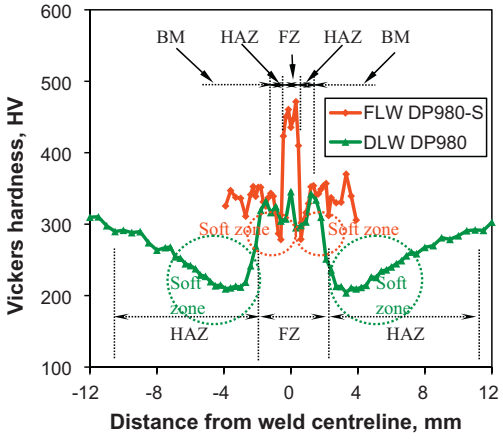

Fig. 4. Hardness profiles across a FLWed DP980-S and a DLWed DP980 joint.

Table 2
Tensile properties, joint efficiency, and fatigue parameters σ'_f and b for the DP980 BM, DLWed DP980 joints, FLWed DP980-S joints, and FLWed DP980-M joints.

Welding type	Yield strength (MPa)	Ultimate tensile strength (MPa)	Elongation (%)	Joint efficiency (%)	Fatigue limit (MPa)	Fatigue ratio	σ'_f (MPa)	b
BM DP980	720	1095	14.2	–	250	0.228	1019	−0.098
DLW DP980	505	724	7.6	66.1	150	0.207	456	−0.054
FLW DP980-S	719	1048	4.6	95.7	150	0.143	1169	−0.132
FLW DP980-M	717	1066	5.1	97.3	<150	0.141	1984	−0.185

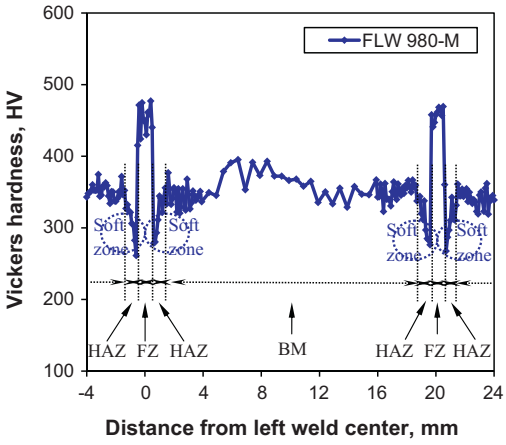

Fig. 5. Hardness profile across a FLWed DP980-M joint.

two FZ pylons. It would be of interest to see if these multiple soft zones would affect tensile and fatigue behavior of the FLWed joint.

3.3. Tensile properties

Fig. 6 demonstrates the typical engineering stress versus engineering strain plots of the BM DP980, DLWed DP980 joint, FLWed DP980-S joint, and FLWed DP980-M joint tested at a strain rate of 1×10^{-3} s^{-1}. It is seen that while the strain to failure was lower, the YS after FLW remained very close to that of BM 980 steel. However, the YS after DLW decreased remarkably. The evaluated tensile test results are listed in Table 2. The YS and UTS of the DLWed DP980 joint were obtained to be an average of 505 MPa and 724 MPa, respectively, which were much lower than those of the BM having a YS of 720 MPa and a UTS of 1095 MPa. Interestingly, the tensile properties of both FLWed DP980-S joint (YS = 719 MPa; UTS = 1048 MPa) and FLWed DP980-M joint (YS = 717 MPa, UTS = 1066 MPa) were very close to the values of the BM, and no obvious difference of the tensile properties between the FLWed DP980-S and DP980-M joints was observed. The joint efficiency reached as high as about 96–97% (Table 2), where the joint efficiency is normally defined as a ratio of the UTS of welded joints to the UTS of the corresponding BM [38–40]. Indeed, if one considers a ratio of the YS of welded joints to the YS of the corresponding BM, then the ratio would arrive at nearly 100%. Thus, it could be concluded that the FLWed joint had a significantly higher tensile performance than the DLW and was nearer almost to that of the BM. It was ascribed to the higher welding speed (Table 1) and lower heat input in the FLW which greatly reduced the detrimental influence of the soft zone by narrowing it down significantly compared to the DLW which resulted in a wider soft zone (Figs. 2(a) and 4). The narrower HAZ was better restrained by the neighboring material which restricted thinning [46].

On the contrary, ductility of both the DLWed joint and the FLWed joints was lower than that of the BM. This was due to the fact that yielding occurred first in the soft zones and the subsequent plastic deformation was predominantly concentrated there. This led in turn to a reduction in the overall specimen elongation, as necking and failure were observed to occur in the soft zone. Similar results were reported in a study of formability of DLWed DP980 and HSLA steels [30,42]. This would also explain the higher ductility in the DLW where the wider soft zone (Figs. 2(a) and 4) could accommodate larger strain before failure compared to the narrower soft zone in FLW (Figs. 3(a) and 4). It was also due to premature failure induced by the soft zone (i.e., lower ductility) that the UTS of FLWed joints became lower (Fig. 6), although a high joint efficiency of about 96–97% was achieved.

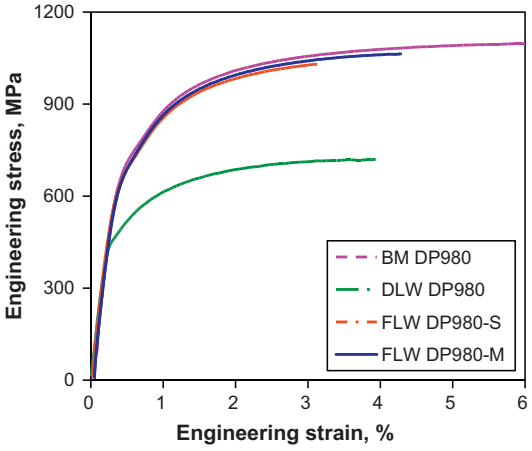

Fig. 6. Representative engineering stress versus engineering strain of the DP980 BM, DLWed DP980 joint, FLWed DP980-S joint, and FLWed DP980-M joint tested at a strain rate of 1×10^{-3} s^{-1}.

3.4. Fatigue strength and failure mode

Fatigue test results of the BM DP980, DLWed DP980 joints, FLWed DP980-S joints and FLWed DP980-M joints obtained at $R = 0.1$, 50 Hz, and room temperature (RT) are plotted in Fig. 7. The DLWed DP980 joints were found to have a much lower fatigue life

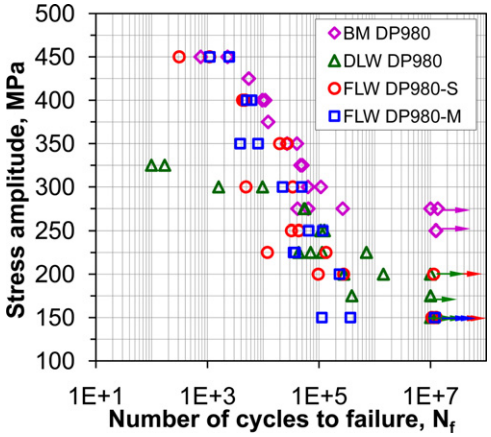

Fig. 7. *S–N* curves of the DP980 BM, DLWed DP980 joints, FLWed DP980-S joints, and FLWed DP980-M joints tested at $R = 0.1$, 50 Hz, and RT.

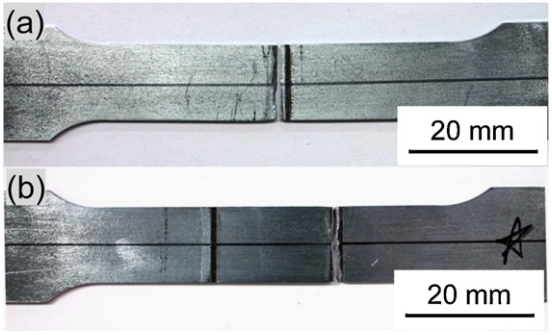

Fig. 8. Typical fatigue failure locations of (a) a FLWed DP980-S joint, and (b) a FLWed DP980-M joint.

or fatigue strength than the BM at both high and low levels of stress amplitudes. For example, the fatigue strength at 1×10^7 cycles (sometimes called conditional fatigue limit) was about 100 MPa lower in the DLWed DP980 joints than the BM, while it was further lower (~150 MPa) in the low cycle fatigue region at 2×10^3 cycles. This corresponded well to the effect of the wider soft zone with significantly lower values in both hardness (Fig. 4) and tensile strength (Fig. 6 and Table 2). The FLWed-DP980 joints exhibited an equivalent or only slightly lower fatigue life than the BM at a stress amplitude above 300 MPa, whereas the fatigue strength of FLWed joints became lower and more scattered below a stress amplitude of 300 MPa. This indicated that while the narrower HAZ-softening (Figs. 3(a), 4 and 5) did not affect the static tensile properties (Fig. 6 and Table 2), the dynamic fatigue resistance was still susceptible to the presence of soft zone, irrespective of the size of soft zones. This observation corresponded well to that reported by Roesler et al. [47] who noted that the fatigue strength of a material under dynamic cyclic loading was much more sensitive to the manufacturing process and materials than the static strength, and that the fatigue strength was also much more sensitive to the lower level cyclic load than the higher level cyclic load. Indeed, in the region of lower level of stress amplitude and longer life, the factors like surface conditions, residual stresses, localized stress concentration, surface protective coating, severe weld concavity and zinc inclusions in weldment are detrimental to fatigue life [29,48]. The fatigue data plotted in Fig. 7 for the multiple linear welds exhibited a larger scatter and lower fatigue strength (e.g., two samples failed at 150 MPa), indicating that the probability of dynamic fatigue failure at the lower level of stress amplitudes increased with increasing number of soft zones.

The fatigue limit and fatigue ratio are tabulated in Table 2. The fatigue limit of both the DLWed DP980 joints and FLWed DP980 joints were obtained to be 150 MPa, which was 40% lower than that of the base metal, and the fatigue ratio (i.e., a ratio of fatigue limit to the UTS) of the DLWed DP980 joints and the FLWed DP980 joints were 0.21 and 0.14, respectively. The lower fatigue ratio of

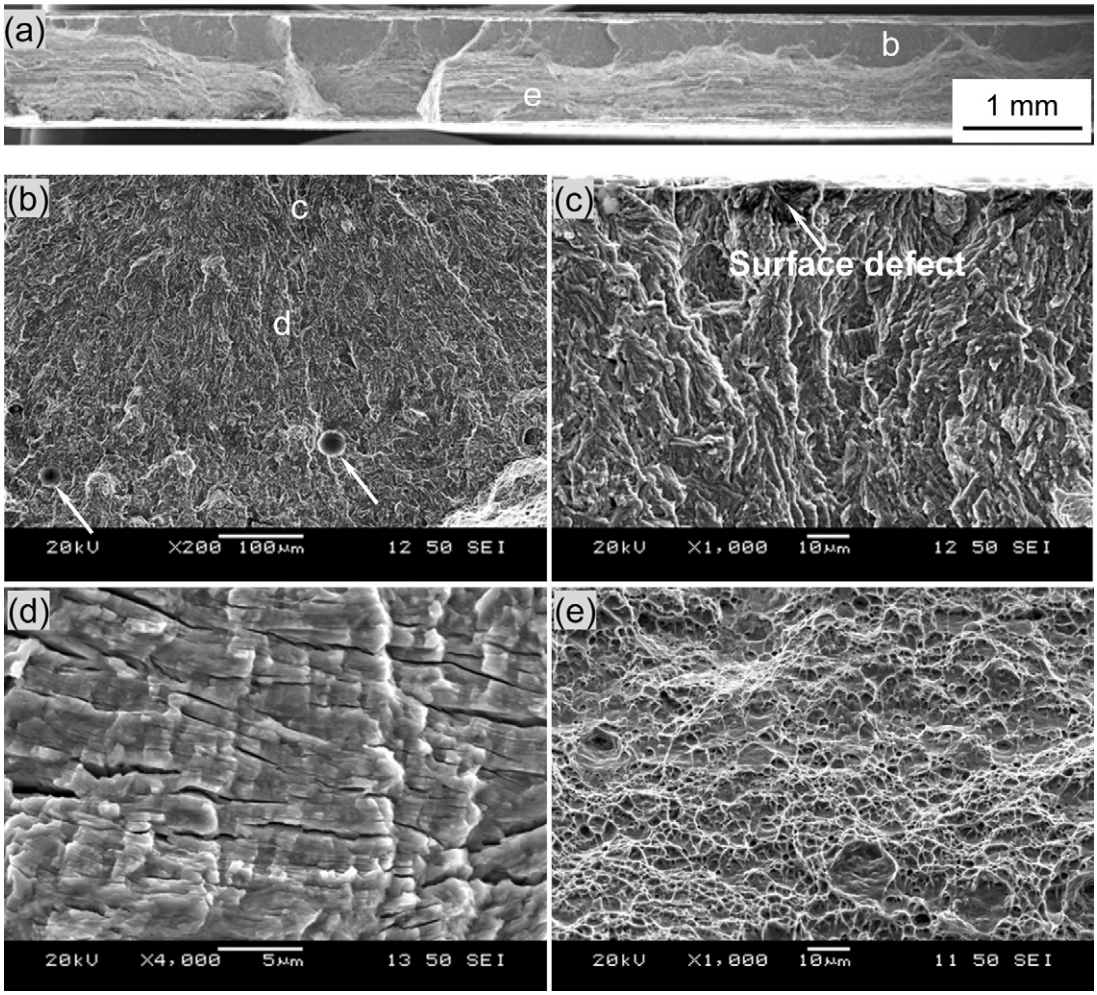

Fig. 9. Typical SEM images of fatigue fracture surface of a FLWed DP980-S joint tested at a stress amplitude of 350 MPa, (a) overall view, (b) fracture surface at a larger magnification, (c) crack initiation area, (d) crack propagation area, (e) final fast propagation area.

FLWed DP980 joints was related to the higher UTS (Table 2). These results suggested that while the tensile strength of the FLWed joints greatly improved, the fatigue strength only improved at a higher level of stress amplitudes (>300 MPa), and was equivalent to that of the DLWed joints at a lower level of stress amplitudes (<300 MPa). One more factor for the low fatigue limit or fatigue ratio in both types of FLWed DP980 joints was associated with the notch effect of weld concavity, since fatigue is a type of notch-sensitive dynamic failure. As seen in Fig. 3(a), the FLW "notch" or weld concavity was similar to a notched specimen (e.g., in [49]) where the stress concentration was generated. As a consequence, this would result in a decreased fatigue limit or fatigue life at the low level of stress amplitudes, stemming from the presence of fatigue notch sensitivity.

The obtained fatigue data shown in Fig. 7 could be further fitted using the following Basquin type equation,

$$\sigma_a = \sigma_f'(2N)^b \quad (1)$$

where σ_a is the stress amplitude, σ_f' is the fatigue strength coefficient defined by the stress intercept at $2N_f = 1$, N_f is the number of cycle to failure, and b is the fatigue strength exponent. The obtained values of σ_f' and b of the base metal, the DLWed DP980 joints and the FLWed DP980 joints tested at $R = 0.1$, 50 Hz and room temperature are given in Table 2, where the fatigue life at a given stress amplitude was dependent on both fatigue strength coefficient σ_f' and fatigue strength exponent b.

3.5. Fractography

The fatigue failure locations for the FLWed DP980-S and FLWed DP980-M joints are shown in Fig. 8. Fatigue failure of all test samples was observed to occur predominantly at the HAZ soft zones. It was less likely to occur at the center of FZ due to the strong FZ hardness "pylon" effect in the FLW (Figs. 4 and 5). The failure location of the FLWed joints was similar to that of the DLWed DP980 joints in which all the fatigue failure also occurred at the soft zones as reported in our earlier study [19]. SEM images of fatigue fracture surface of a FLWed DP980-S joint tested at an applied stress amplitude of 350 MPa are shown in Fig. 9. It is seen from Fig. 9(a) that multiple crack initiation occurred from the surface where the weld concavity met with the soft zone. The magnified SEM images on some features near a crack initiation site are shown in Fig. 9(b) and (c), where some gas pores trapped during FLW (Fig. 9(b)) and surface welding defects (Fig. 9(c)) could be seen, as indicated by arrows on the images. These were similar to fatigue fracture surface features reported for a FLWed AZ31B-H24 Mg alloy [40]. The fatigue crack initiation in the present FLWed DP980 steel would mainly be related to the severe weld concavity (Fig. 3(a)) and the ensuing stress concentration, and the presence of soft zones (Figs. 4 and 5). Fatigue crack propagation was mainly characterized by fatigue striations in conjunction with secondary cracks, as shown in Fig. 9(d), while the final fast propagation area consisted of characteristic dimples. The spacing of fatigue striations increased with increasing distance from the crack initiation site, reflecting a gradually increasing fatigue crack propagation rate. Fatigue striations basically occurred via a repeated plastic blunting-sharpening process via the slip of dislocations in the plastic zone ahead of the fatigue crack tip [50].

4. Conclusions

The microstructure, hardness profile, tensile properties and fatigue performance of single linear and multiple linear joints of DP980 dual-phase steel made by FLW process were presented and the results were compared with those of DLWed DP980 joints in the present study. The following conclusions could be drawn:

1. Both DLWed and FLWed joints showed tempered martensite at the outer HAZ which caused softening in the welds. More complete martensite tempering or decomposition occurred in the HAZ of the DLWed joint than in the HAZ of the FLWed joint due to a lower welding speed and more heat input.
2. While the microstructure in the FZ of DLWed joints consisted mainly of martensite, ferrite, and bainite, almost fully martensitic structure was observed in the FZ of FLWed joints due to a faster cooling rate. This led to a characteristic "suspension bridge"-like hardness profile with the FZ hardness as a "pylon" in the FLW.
3. The FLWed joints had a much narrower soft zone with a higher hardness due to a higher welding speed and lower degree of martensite tempering, in comparison with the DLWed joints. This resulted in a higher ultimate tensile strength with a joint efficiency reaching as high as 96–97% while the yield strength was essentially unaffected and ductility became lower.
4. At a higher stress amplitude above 300 MPa, fatigue life of the FLWed joints was equivalent to that of BM, while FLW did not result in an improved fatigue performance at a lower stress amplitude below 300 MPa in comparison with the DLWed joints, because the dynamic fatigue resistance was susceptible to the presence of soft zone and the weld concavity-induced fatigue notch sensitivity. The multiple linear welds appeared to increase the probability of dynamic fatigue failure at a lower level of stress amplitudes due to an increasing number of weld concavities and soft zones present.
5. Fatigue crack initiation was observed to occur from the specimen surface where the weld concavity met with a soft zone, and crack propagation was characterized by the characteristic fatigue striations coupled with secondary cracks for all types of the welded joints.

Acknowledgements

The authors would like to thank the Natural Sciences and Engineering Research Council of Canada (NSERC) and AUTO21 Network of Centers of Excellence for providing financial support. The financial support from International Zinc Association (IZA) and ArcelorMittal Dofasco is highly acknowledged. One of the authors (D.L. Chen) is grateful for the financial support by the Premier's Research Excellence Award (PREA), NSERC-Discovery Accelerator Supplement (DAS) Award, Canada Foundation for Innovation (CFI), and Ryerson Research Chair (RRC) program. The authors would like to thank Dr. J. Chen and Dr. Y.L. He (CANMET-Materials Technology Laboratory, Natural Resources Canada), and Dr. J. Villafuerte (CenterLine (Windsor) Ltd.) for their support and helpful discussion. The assistance of Q. Li, A. Machin, J. Amankrah, and R. Churaman in performing the experiments is gratefully acknowledged.

References

[1] J. Nilsson, D.N. Payne, Science 332 (2011) 921–922.
[2] C.P. Christensen, Science 224 (1984) 117–123.
[3] C.P. Christensen, Science 218 (1982) 115–121.
[4] S. Daneshpour, S. Riekehr, M. Kocak, C.H.J. Gerritsen, Sci. Technol. Weld. Join. 14 (2009) 20–25.
[5] L. Quintino, A. Costa, R. Miranda, D. Yapp, V. Kumar, C.J. Kong, Mater. Des. 28 (2007) 1231–1237.
[6] K. Sripichai, K. Asim, J. Pan, Eng. Fract. Mech. 78 (2011) 1424–1440.
[7] E. Ahmed, U. Reisgen, M. Schleser, O. Mokrov, Sci. Technol. Weld. Join. 15 (2010) 337–342.
[8] C.H. Kim, J.K. Choi, M.J. Kang, Y.D. Park, J. Achiev. Mater. Manuf. 39 (2010) 79–86.
[9] R. Term, Weld. Des. Fabr. 2 (2001) 37–40.
[10] G. Overton, Laser Focus World 10 (2008) 90–93.
[11] F.I. Saunders, R.H. Wagoner, Metall. Mater. Trans. A 27A (1996) 2605–2616.

[12] L.C. Chan, C.H. Cheng, S.M. Chan, T.C. Lee, C.L. Chow, J. Manuf. Sci. Eng. 127 (2005) 743–751.
[13] D. Anand, G. Boudreau, P. Andreychuk, D.L. Chen, S.D. Bhole, Can. Metall. Q. 45 (2005) 189–198.
[14] K.B. Min, S.S. Kang, J. Mater. Process. Technol. 103 (2000) 218–224.
[15] C. Ma, D.L. Chen, S.D. Bhole, G. Boudreau, A. Lee, E. Biro, Mater. Sci. Eng. A 485 (2008) 334–346.
[16] S.D. Bhole, C. Ma, M.S. Khan, D.L. Chen, J. Iron Steel Res. Int. 18 (Suppl. 1, Part 2) (2011) 724–729.
[17] C. Ma, S.D. Bhole, D.L. Chen, A. Lee, E. Biro, G. Boudreau, Sci. Technol. Weld. Join. 11 (2006) 480–487.
[18] M.S. Khan, S.D. Bhole, D.L. Chen, G. Boudreau, E. Biro, J.V. Deventer, Can. Metall. Q. 48 (2009) 303–310.
[19] M.S. Khan, S.D. Bhole, D.L. Chen, G. Boudreau, E. Biro, J.V. Deventer, Sci. Technol. Weld. Join. 14 (2009) 616–625.
[20] N. Farabi, D.L. Chen, Y. Zhou, J. Alloys Compd. 509 (2011) 982–989.
[21] N. Sreenivasan, M. Xia, S. Lawson, Y. Zhou, J. Eng. Mater. Technol. 130 (2008) 0410041–0410049.
[22] X. Sun, K.S. Choi, A. Soulami, W.N. Liu, M.A. Khaleel, Mater. Sci. Eng. A 526 (2009) 140–149.
[23] M. Xia, E. Biro, Z. Tian, Y. Zhou, ISIJ Int. 48 (2008) 809–814.
[24] W. Bleck, JOM 48 (1996) 26–30.
[25] M.S. Xia, M.L. Kuntz, Z.L. Tian, Y. Zhou, Sci. Technol. Weld. Join. 13 (2008) 378–387.
[26] N. Farabi, D.L. Chen, Y. Zhou, J. Mater. Eng. Perform. 21 (2012) 222–230.
[27] N. Farabi, D.L. Chen, Y. Zhou, Procedia Eng. 2 (2010) 835–843.
[28] N. Farabi, D.L. Chen, J. Li, Y. Zhou, S.J. Dong, Mater. Sci. Eng. A 527 (2010) 1215–1222.
[29] D. Anand, D.L. Chen, S.D. Bhole, P. Andreychuk, G. Boudreau, Mater. Sci. Eng. A 420 (2006) 199–207.
[30] M. Xia, N. Sreenivasan, S. Lawson, Y. Zhou, Z. Tian, Trans. ASME 129 (2007) 446–452.
[31] P. Hill, Opt. Laser Europe 9 (2002) 7–8.
[32] U. Reisgen, M. Schleser, O. Mokrov, E. Ahmed, Opt. Laser Technol. 44 (2012) 255–262.
[33] E.L. Guen, M. Carin, R. Fabbro, F. Coste, P.L. Masson, J. Inter, Heat Mass Transfer 54 (2011) 1313–1322.
[34] K. Gilles, Weld. Des. Fabr. 79 (2006) 24–25.
[35] L. Commin, M. Dumont, R. Rotinat, F. Pierron, J.-E. Masse, L. Barrallier, Mater. Sci. Eng. A 528 (2011) 2049–2055.
[36] A.K. Dasgupta, J. Mazumder, Sci. Technol. Weld. Join. 13 (2008) 289–293.
[37] K. Asim, J. Lee, J. Pan, Fatigue Fract. Eng. Mater. Struct. 35 (2010) 219–237.
[38] S.M. Chowdhury, D.L. Chen, S.D. Bhole, E. Powidajko, D.C. Weckman, Y. Zhou, Metall. Mater. Trans. A 42 (2011) 1974–1989.
[39] S.M. Chowdhury, D.L. Chen, S.D. Bhole, X. Cao, E. Powidajko, D.C. Weckman, Y. Zhou, Mater. Sci. Eng. A 527 (2010) 2951–2961.
[40] S.H. Chowdhury, D.L. Chen, S.D. Bhole, E. Powidajko, D.C. Weckman, Y. Zhou, Metall. Mater. Trans. A, http://dx.doi.org/10.1007/s11661-011-1042-z, in press.
[41] T. Huang, Y.S. Sato, H. Kokawa, M.P. Miles, K. Kohkonen, B. Siemssen, R.J. Steel, S. Packer, Metall. Mater. Trans. A 40 (2009) 2994–3000.
[42] S.K. Panda, V.H. Baltazar, Hernandez, M.L. Kuntz, Y. Zhou, Metall. Mater. Trans A 40 (2009) 1955–1967.
[43] E. Biro, J.R. McDermid, J.D. Embury, Y. Zhou, Metall. Mater. Trans A 41 (2010) 2348–2356.
[44] V.H.B. Hernandez, S.S. Nayak, Y. Zhou, Metall. Mater. Trans A 42 (2011) 3115–3129.
[45] S. Kou, Welding Metallurgy, 2nd ed., Hoboken, John Wiley & Sons, Inc., 2003, pp. 291–308.
[46] S.K. Panda, N. Sreenivasan, M.L. Kuntz, Y. Zhou, J. Eng. Mater. Technol. 130 (2008), 041003-1–9.
[47] J. Roesler, H. Harders, M. Baeker, Mechanical Behavior of Engineering Materials: Metals, Ceramics, Polymers, and Composites, 1st ed., Springer Publication, 2007, pp. 499–535.
[48] R.S. Sharma, P. Molian, Mater. Des. 30 (2009) 4146–4155.
[49] M.D. Chapetti, N. Katsura, T. Tagawa, T. Miyata, Int. J. Fatigue 23 (2001) 207–214.
[50] C. Laird, Fatigue Crack Propagation, ASTM Spec. Tech. Publ., 415, West Conshohocken, PA, 1967.